Journal of Applied Polymer Science

Investigation on enhancement of weld strength between PMMA and PBT in laser transmission welding—Using intermediate material

Xiao Wang, Xuejiao Zhong, Wei Liu, Baoguang Liu, Huixia Liu
School of Mechanical Engineering, Jiangsu University, Zhenjiang 212013, China
Correspondence to: X. Wang (E-mail: wx@ujs.edu.cn)

ABSTRACT: Poly(methyl methacrylate) (PMMA) and poly(butylene terephthalate) (PBT) are widely used in industry; however, poor compatibility between two materials lead to poor weld strength. Polycarbonate (PC) has good compatibility with PMMA and PBT. Therefore, the welding method was that PC film as intermediate material was used to enhance weld strength in laser transmission welding (LTW) of PMMA and PBT. Through the LTW experiment, the weld strength was tested by mechanical testing and it was found that the best weld strength was improved more than four times than the weld strength without intermediate material. By observing the micro morphology of the weld zone, one reason was founded that the bubbles can be used to form micro-mechanical riveting to enhance the weld strength. The reptation time for PMMA, PC, and PBT were investigated to analyze the establishment of the weld strength. When the reptation time is much shorter than time in molten state, the higher weld strength is feasible. It can be concluded that the weld strength of PC/PBT was higher than the weld strength of PMMA/PC. The equilibrium interfacial width was calculated through Helfand's theory to analyze the compatibility of dissimilar materials. The equilibrium interfacial width for PMMA/PC and PC/PBT were similar to tube diameter. That is the reason for weld strength enhancement. And then, the response surface methodology was designed to predict the weld strength.© 2016 Wiley Periodicals, Inc. J. Appl. Polym. Sci. **2016**, *133*, 44167.

KEYWORDS: differential scanning calorimetry; mechanical properties; surfaces and interfaces; thermoplastics

Received 1 April 2016; accepted 7 July 2016
DOI: 10.1002/app.44167

INTRODUCTION

The products of connecting dissimilar polymers are widely used in the fields of microelectronics, medical industries and automobile parts.[1–3] The connection of dissimilar materials can combine the excellent properties of the two materials, but it is more difficult than the connection of the same material. The major traditional methods of connecting dissimilar materials are adhesive bonding, friction welding, hot plate welding, and so on. These methods play important roles in different fields; however, they have some disadvantages, such as low welding efficiency, poor welding quality and so on.[4] Comparing with traditional welding methods, laser transmission welding (LTW) has many advantages, such as no contact, high speed, high precision, flexibility, small heat affected zone and so on.[5–7]

In recent years, there are many studies on LTW dissimilar polymer materials. Anssi *et al.*[8] used contour welding and simultaneous welding to analyze the effect of process parameters on the welding quality during the process of LTW polycarbonate (PC) and PC/acrylonitrile butadiene styrene (ABS) blend. Aden *et al.*[9] used a new method of transmission welding incremental scanning technique (TWIST) welding method to weld polyamide 66 (PA66) and Polypropylene (PP). It was found that this method can obtain more uniform welding seam and higher weld strength. Acherjee *et al.*[10] studied on LTW of PC and ABS. The mathematical model based on response surface method was established to discuss the influence of laser power, scanning speed, defocusing amount, and clamping force on welding quality. At present, the study of LTW dissimilar materials which can be weld original mainly focused on optimization of experimental parameters, but there are few studies of LTW dissimilar materials which cannot be weld well at first. Liu *et al.*[11] improved the welding performance in LTW PP and PA66 through the using maleic anhydride grafted the side chains of PP. It was founded that the weld strength greatly improved. Liu *et al.*[12] sprayed a 20 μm thick aluminum film on glass fiber-reinforced polyamide 66 (GFR-PA66) to improve the weld strength between GFR-PA66 and PC. The results showed that the weld strength can reach about 4 MPa. However, the method of modifying the material may change some properties of the material, and coating metal film on the surface of the material has relatively high cost.

Poly(methyl methacrylate) (PMMA) a kind of amorphous polymer, because of its excellent light transmission properties, good chemical resistance, solvent resistance, heat and cold resistance,

is widely used in automotive, advertising, medical, communications and construction and other fields.[13] Poly(butylene terephthalate) (PBT) a kind of semicrystalline polymer, due to its excellent mechanical properties and processing performance, especially good comprehensive performance, is widely used in industry.[14] If PMMA and PBT can be welded together by LTW, their respective advantages will be fully utilized and will have great prospects of application. But the two materials have poor compatibility; and the weld strength of welding materials is poor.[15,16] PC has good compatibility with PMMA and PBT.[17,18] In this study, the method of LTW was that the PC film as an intermediate material was used to enhance weld strength in LTW of PMMA and PBT. This method cannot change properties of the material and has relatively low cost. In order to analyze the welding performance of specimens with or without adding intermediate material, the tensile tests were carried out and the micro morphology of weld zone was observed by optical microscope. Furthermore, the influence of and reptation time (τ_{rep}) for PMMA, PC, and PBT on welding performance was investigated. The equilibrium interfacial width (w_∞) was calculated by Helfand's theory to analyze the compatibility of materials and the reason of strength enhancement.

The process parameters also have great influence on the weld strength of LTW polymers. To find the best process parameters need a large of experiments in industrial applications. Therefore, it is important to analyze the process parameters on weld strength. The response surface methodology (RSM) of experimental design is one of the best known optimization tools, which can analyze of experiments with least experimental effort.[19] RSM is widely used to predict the weld seam and mechanical models in different welding processes. In this study, RSM was developed to predict the weld strength of LTW PMMA and PBT with intermediate material.

THEORY

Polymer Miscibility

Polymer–polymer miscibility is an important criterion for mutual diffusion of polymers, that is to say the ability of mixing two polymers together and being in one phase at thermodynamic equilibrium.[20] Compatibility plays an important role in LTW dissimilar materials. The thermodynamic compatibility can be expressed by[21]:

$$\Delta G = \chi \cdot \varphi_1 \cdot \varphi_2 + \frac{\varphi_1}{N_1} \cdot \ln \varphi_1 + \frac{\varphi_2}{N_2} \cdot \ln \varphi_2 \quad (1)$$

where ΔG is Gibbs free energy, χ is the Flory–Huggins interaction parameter, N_i is the degree of polymerization of component number i, φ_i is the volume fraction of component number i, and $\varphi_1 + \varphi_2 = 1$.

$\Delta G < 0$ is a necessary condition to meet thermodynamic compatibility, i.e., the two kinds of polymer can be considered fully compatible, and the molecules can be completely mixed. The latter two terms of eq. (1) are less than zero, because $0 < \varphi_1 < 1$ and $0 < \varphi_2 < 1$. The latter two terms of eq. (1) are almost zero, because the degree of polymerization is very big ($10^4 \sim 10^6$g/mol). Therefore, the size of ΔG depends on the first term of eq. (1) and χ parameter is an important factor for ΔG. The χ parameter can be estimated by Hansen solubility parameters[22]:

$$\chi = \frac{V_m \cdot ((\delta_{D1} - \delta_{D2})^2 + 1/4(\delta_{P1} - \delta_{P2})^2 + 1/4(\delta_{H1} - \delta_{H2})^2)}{RT} \quad (2)$$

where δ_D, δ_P, and δ_H, respectively represent the dispersion component, dipole component and hydrogen bond component of Hanson solubility parameters ($J^{1/2}\,m^{-3/2}$). V_m is the molar volume (cm^3/mol). The molar volume of the two polymer system is given as the geometric mean ($\sqrt{V_{m1} \cdot V_{m2}}$). R is ideal gas constant, and the value is 8.314 J/(mol K). T is absolute temperature (K).

The χ parameter is usually greater than zero.[23] The ΔG is greater than zero for dissimilar materials. So the intermolecular of most dissimilar polymers cannot be completely mixed, i.e., the phases of dissimilar polymers cannot form a homogeneous system. But, being not fully compatible does not mean being incompatible. The transition layer is formed between two different phases. The width of transition layer is called equilibrium interfacial width (w_∞). Under the condition of equilibrium, two kinds of molecular chain and chain segment in this transition layer form an entanglement network by a series of thermal motion (entanglement, disentanglement and reentanglement). The width of the transition layer directly reflects the degree of compatibility between different polymers. The compatibility between different polymers is better, i.e., the degree of the inter diffusion between the molecular chains of two polymers is higher and the transition layer is wider.[21] It is beneficial to interact between molecular chains and the establishment of weld strength during the LTW.

The equilibrium interfacial width can be estimated from Helfand's theory[24,25]:

$$w_\infty = 2 \cdot \sqrt{\frac{b_I^2 + b_{II}^2}{12 \cdot \chi}} \quad (3)$$

where b_i (where is number I or number II) is the statistical segment length of polymer i (nm).

For strength development at the interface, not only is the equilibrium interfacial width important but also is the entanglement mesh spacing of the polymer. If the mesh size is large, polymer interface needs a large equilibrium interfacial width to ensure entanglements. And, vice versa, if the mesh size is small, entanglements can easily occur.[21] Usually, entanglement mesh size is equal to the tube diameter (a). So, a measurement of the entanglement mesh size is the tube diameter.[26]

Reptation Model

The reptation model is the most common method for studying the entanglement of the molecular chains. This model dates back to de Gennes,[27] who was the first to propose polymer dynamics caused by reptation mechanisms. Molecular chain movement in the constricted chain tube is realized through the diffusion of the chain segment along the original path. The constricted tube is made up of other molecular chains and itself also in moves and changes. At first, the molecular chain is constricted in tube. Then the constricted tube starts to change and the molecular chain is wriggle and diffusion under

external force. After a long period of external force, the molecular chain eventually escape the initial constricted tube to a new constricted tube, and the initial tube disappeared. The time it takes to escape the tube is defined as reptation time (τ_{rep}), and therefore during reptation time a polymer chain has diffused one radius of gyration, R_g.[28] The weld strength between dissimilar polymers can be formed through LTW. If τ_{rep} is small, the time of molecular chain completing a series of process of diffusion, peristalsis, disentanglement and regenerate entanglement is short. It is beneficial to interaction between molecular chains and the establishment of weld strength during the LTW.[29]

Later Edwards and Doi studied the relationship between macroscopic zero shear viscosity (η_0) and microscopic reptation time (τ_{rep}). The expression of equation as follows[30]:

$$\eta_0 = \frac{\pi^2 c k_B T}{20 N_e} \tau_{rep} \tag{4}$$

To determine the reptation time, it is also noticeable that it depends linearly on η_0, which varies with temperature. Therefore eq. (4) can be rewritten to:

$$\tau_{rep}(T) = \frac{20 N_e}{\pi^2 c k_B T} \eta_0(T) = \frac{20 M_e}{\pi^2 R T \rho} \eta_0(T) \tag{5}$$

where c is the number density of monomers, and therefore equals $\rho N_A / M_0$, where ρ is the melt density and M_0 is the monomer molecular weight. $M_e = N_e M_0$ is the molecular weight between entanglements, N_e is the number of monomers between entanglements, $R = k_b N_A$ is the gas constant, k_B is Boltzmann's constant.

The zero shear viscosity and temperature meets the condition of Arrhenius equation[26]:

$$\eta_0(T) = K e^{E_\eta / RT} \tag{6}$$

where K is material constant, E_η is the activation energy for flow. The eq. (6) can be simplified:

$$\eta_0(T) = A e^{B/T} \tag{7}$$

where A and B are constants. Therefore eq. (5) can be rewritten to:

Table I. Process Parameters for Injection Molding

Polymer	PMMA	PBT
Drying time (h)	4	4
Drying temp. (°C)	80	120
Extruding temp. (°C)	245	250
Screw speed (r/min)	30	60
Inj. molding melt temp (°C)	255	260
Tool temp. (°C)	60	60
Cooling time (s)	20	20
Holding press. (MPa)	50	4
Holding time (s)	2	30

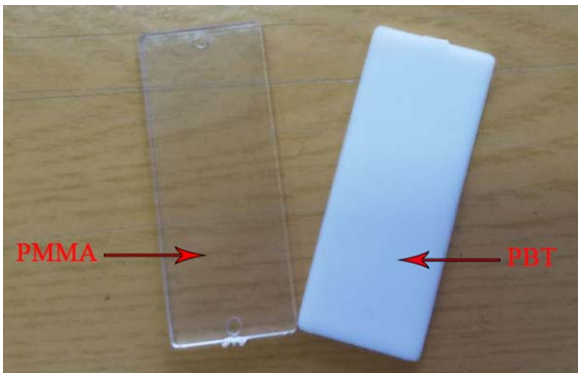

Figure 1. The samples of PMMA and PBT. [Color figure can be viewed in the online issue, which is available at wileyonlinelibrary.com.]

$$\tau_{rep}(T) = \frac{20 M_e}{\pi^2 R T \rho} \eta_0(T)^{0 = \frac{20 M_e}{\pi^2 R T \rho} A e^{B/T}} \tag{8}$$

Response Surface Method

Response surface method is a combination of mathematical statistics and design of experiment that is used to model and analyze of problems in which a response of interest is restricted by several variables. In most of the response surface optimization problem, a suitable function relation approach is needed to find a suitable function between the response variables y and the independent variables $(x_1, x_2, \ldots, x_k)$. If all variables are assumed to be measurable, the response surface can be expressed as follows[19]:

$$y = f(x_1, x_2, \ldots, x_k) + \varepsilon \tag{9}$$

where ε is the response system error, the value is usually assumed zero, the variance is σ^2.

Therefore, a second order polynomial equation is used in RSM:

$$y = \beta_0 + \sum_{j=1}^{k} \beta_j x_j + \sum_{j=1}^{k} \beta_{jj} x j^2 + \sum_{i<j} \sum_{j=2}^{k} \beta_{ij} x_i x_j \tag{10}$$

where y is the response, k is the number of model inputs, x_i, x_j are called the set of model input variables (design variables), β_0, β_j, β_{jj}, β_{ij} are called the polynomial coefficients.

EXPERIMENTAL

Experimental Materials

The materials employed in this study are PMMA (Acrypet® VH001), PBT (Ultradur® B4500), and PC (Dobesty® PC6681 film and sheet). PMMA and PBT were manufactured by injection molding. And the process parameters are given in Table I. The dimension of PMMA and PBT is 20 mm × 50 mm × 1.5 mm. The specimens are shown in Figure 1. The dimension of PC film is 20 mm × 20 mm × 0.125 mm, and the dimension of PC sheet is 20 mm × 50 mm × 1.5 mm. Table II. shows some physics data of PMMA, PC, and PBT. The PMMA was used as upper material in the LTW PMMA/PC, PMMA/PBT, and PMMA/PC/PBT (A/B is represent LTW material A and material B; A/C/B is represent LTW material A, material C, and material B; material A is upper material, material B is lower material, and material C is a film which is used as intermediate material); the PBT was used as lower material in the LTW PC/

Table II. Physics Data of PMMA, PC, and PBT

Symbol	Description	PMMA	PC	PBT
$_b$ (Å)[a]	Statistical segment length	6.24	10.7	5.7
(nm)[b]	Tube diameter	7	3.8	3.5
M_e (g/mol)[b]	Molecular weight between entanglements	10,000	1328	1160
M_O (g/mol)[b]	Monomer molar mass	97.09	254.27	220.22
ρ_{melt} (kg/m^3)[b]	Melt density	1130	1140	1238[d]
δ_D (MPa$^{1/2}$)[c]	Hansen solubility parameters	18.8	19.9	20.3
δ_p (MPa$^{1/2}$)[c]	Hansen solubility parameters	12.8	10.7	5.3
δ_H (MPa$^{1/2}$)[c]	Hansen solubility parameters	4.2	2.0	6.1
V_m (cm^3/mol)[c]	Molar volume	86.5	174.4	143.5

[a] Ref. 28.
[b] Ref. 31.
[c] Ref. 20.
[d] Ref. 32.

PBT, PMMA/PBT, and PMMA/PC/PBT; the PC sheet was used as upper material in LTW PC/PBT and used as lower material in LTW PMMA/PC; the PC film was used as intermediate material in LTW PMMA/PC/PBT. To reduce the influence of water on experiment, a KQ3200E ultrasonic cleaning machine was used for clean the specimens before welding, and then the specimens were placed in a 298.15 K and 20% RH conditions of drying oven about 12 h.

Differential Scanning Calorimetry

Thermal characterization of the materials was done by differential scanning calorimetry (DSC) using a DSC800 from PerkinElmer. All materials were cut into small pieces (3 mg of material). The materials were placed in aluminum pans. All samples were heated at the rate of 10 K/min from 323.15 K to 503.15 K, 503.15 K and 523.15 K for PMMA, PC, and PBT, respectively. The test was performed with N_2 as purge gas and flow rate of the gas was 50 mL/min.

The result of the test is that the glass transition temperature (T_g) of PMMA is 383.24 K, the glass transition temperature of PC is 422.86 K and the melting temperature (T_m) of PBT is 495.09 K.

Rheometry

The viscosity was tested by using AR2000 rheometer with ETC equipment from TA Instruments. The reptation time of the selected PMMA, PC, and PBT is determined from the zero shear viscosity (η_0). In theory of linear Viscoelasticity, the viscosity is independent of shear rate. Molten polymers to approach this behavior at very low shear rates, and the limiting, low-shear-rate value of the viscosity is called the zero shear viscosity.[26] Limited by experimental conditions, when the angular velocity is less than 0.1 rad/s, the value of η_0 is instability. Therefore η_0 was determined as the viscosity at 0.1 rad/s in this study. The relationships of viscosity and angular velocity of three polymers under different temperatures are presented in Figures 2, 3, and 4.

Laser Transmission Welding

In this study, a Compact 130/400 semiconductor continuous laser manufactured by DILAS was used for welding experiments. The maximum power of the laser device is 130 W, the output

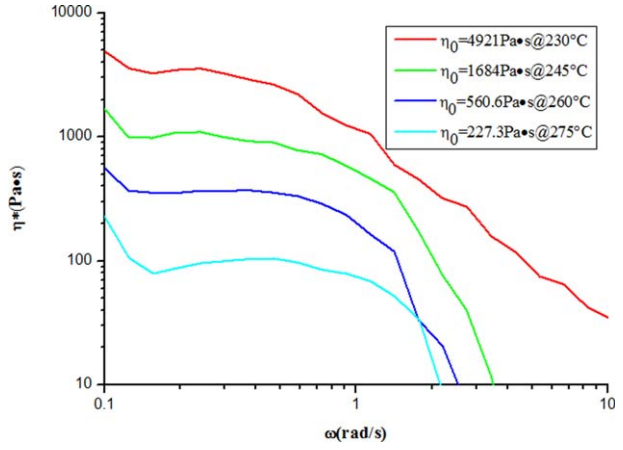

Figure 2. Viscosity versus angular velocity for PMMA. [Color figure can be viewed in the online issue, which is available at wileyonlinelibrary.com.]

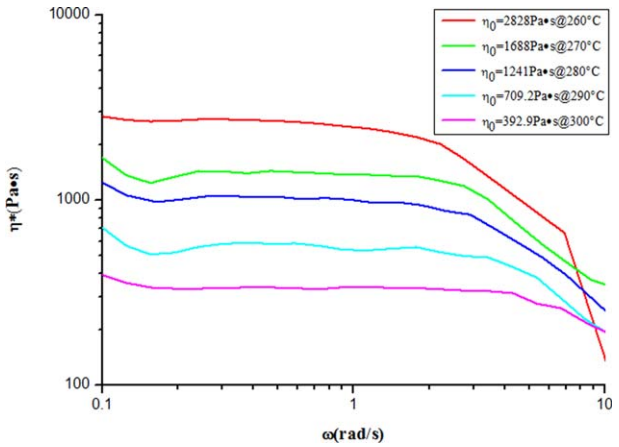

Figure 3. Viscosity versus angular velocity for PC. [Color figure can be viewed in the online issue, which is available at wileyonlinelibrary.com.]

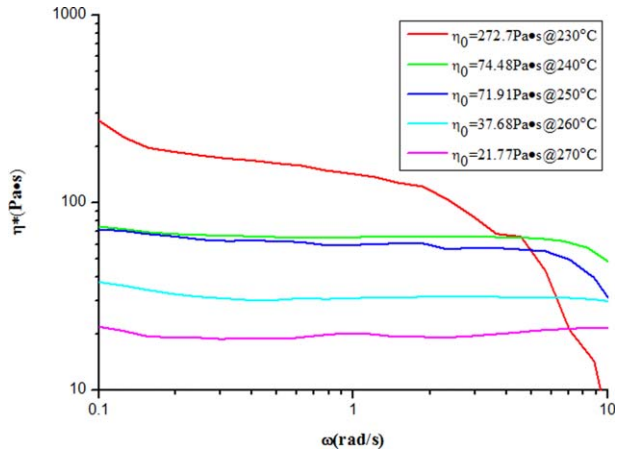

Figure 4. Viscosity versus angular velocity for PBT. [Color figure can be viewed in the online issue, which is available at wileyonlinelibrary.com.]

wavelength is 980 ± 10 nm, the minimum spot diameter is 0.72 mm and the optical fiber transmission is used. K9 glass was used to ensure the uniformity of clamping force. Lap joint was used in the LTW. During LTW, laser need to go through the upper material to the upper surface of the lower material, and the energy of laser was absorbed by the upper surface of the lower material. Then the absorbed energy leaded to melt to two materials, and there was a molten zone in the interface. Under the clamping force, molten materials can be combined by Van Edward force or chemical bonding. Figure 5 is the traditional schematic diagram of LTW. Figure 6 shows another welding method. A film which has good compatibility with both the upper and lower materials was used as intermediate material. Therefore laser need to through upper two materials.

In this study, four groups of LTW experiments were used to compare. They are PMMA/PC, PC/PBT, PMMA/PBT, and PMMA/PC/PBT, respectively. All materials have good transmittance. Therefore, the welding region of lower materials was coated with clear weld as the absorbing layer. In the experiments, the process parameters of spot diameter (0.802 mm), welding speed (4 mm/s), and clamping pressure (0.45 MPa) kept unchanged and this values were chosen from pre-

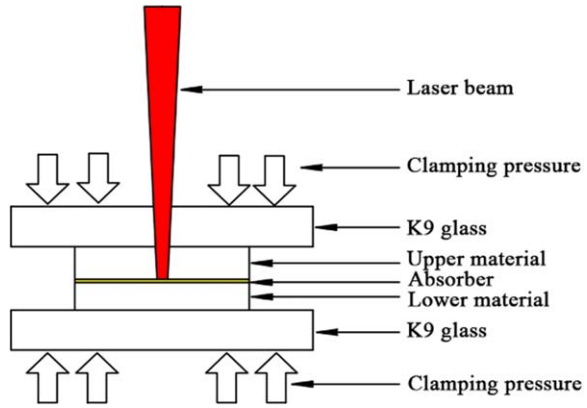

Figure 5. The traditional schematic diagram of LTW. [Color figure can be viewed in the online issue, which is available at wileyonlinelibrary.com.]

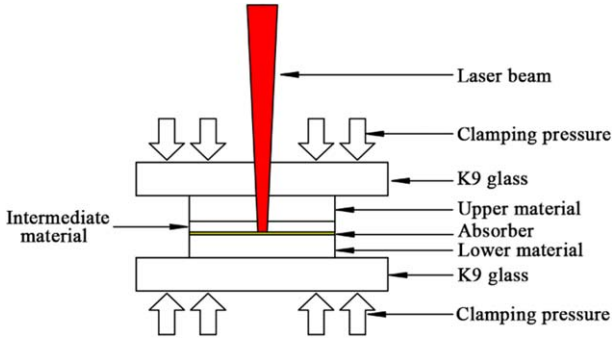

Figure 6. The schematic diagram of LTW with intermediate material. [Color figure can be viewed in the online issue, which is available at wileyonlinelibrary.com.]

experiments; the process of laser powers increased from 15 W to 25 W.

The weld strength is one of important standards to evaluate the quality of the welding. UTM4104 microcomputer control electronic universal testing machine was used to do the tensile tests, and Keyence VHX-1000 ultra-depth electron microscope was used to measure the width of the weld seam.

With tensile speed at 3 mm/min and work environment at room temperature, tensile tests finally break the samples through loading tension at both ends of the samples. The limit stress of the samples can be used to evaluate the weld strength of the samples. The tensile schematic diagram is shown in Figure 7 and the equation for calculating stress[11]:

$$\sigma = \frac{F}{(D \times L)} \tag{11}$$

where σ is the weld strength MPa, F is the maximum pull-off force to make the welding failure (N), D is the width of the weld seam (mm), and L is the length of the weld seam (mm).

RESULTS AND DISCUSSION

Mechanical Testing

The welding specimens of PMMA/PBT and PMMA/PC/PBT when the laser power was 19 W are shown in Figure 8. Figure 8(a) shows the welding specimen of PMMA/PBT and Figure 8(b) shows the welding specimen of PMMA/PC/PBT. From a macro perspective, the two welding specimens are similar and the weld seams are uniform.

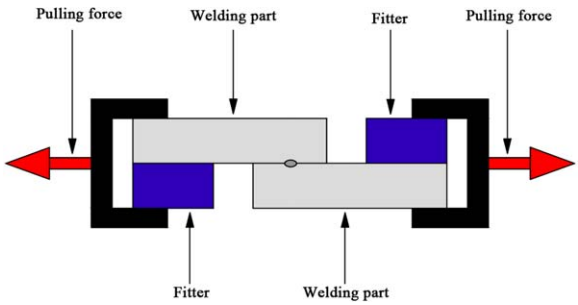

Figure 7. The tensile schematic diagram. [Color figure can be viewed in the online issue, which is available at wileyonlinelibrary.com.]

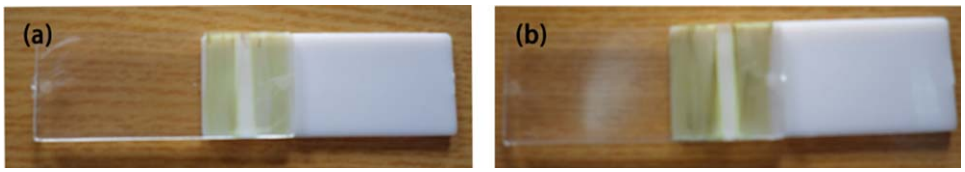

Figure 8. (a) The welding specimen of PMMA/PBT and (b) the welding specimen of PMMA/PC/PBT when the laser power is 19w. [Color figure can be viewed in the online issue, which is available at wileyonlinelibrary.com.]

The specimens after tensile testing are shown in Figure 9, and these specimens are selected with random. Figure 9(a) shows the broken specimen of LTW PMMA/PBT; Figure 9(b) shows the broken specimen of LTW PMMA/PC/PBT. The tensile fracture of LTW PMMA/PBT specimens in the weld seam showed in Figure 9(a); the tensile fracture of LTW PMMA/PC/PBT specimens happened in upper material, and most happened in heat affected zones of PMMA which showed in Figure 9(b).

The tensile results show in Table III. The weld strength is the middle value of the five experiments; the weld width and pulling force were measured from corresponding specimen. The standard deviation in the Table III is the weld strength of five experiments. The specimen numbers from 1 to 6 are used to represent the welding specimens of PMMA/PC; the specimen numbers from 7 to 12 are used to represent the welding specimens of PC/PBT; the specimen numbers from 13 to 18 are used to represent the welding specimens of PMMA/PBT; the sample numbers from 19 to 24 are represent the welding specimens of PMMA/PC/PBT. Comparing the weld strength of PMMA/PC/PBT and PMMA/PBT, when the power is 19 W, the weld strength of PMMA/PC/PBT can reach to 10.04 MPa, while the weld strength of PMMA/PBT only reach to 2.42 MPa; therefore the strength of the specimen PMMA/PC/PBT is more than four times stronger than the strength of specimen PMMA/PBT. At the other power, the weld strength of the specimen PMMA/PC/PBT is two to four times stronger than the weld strength of specimen PMMA/PBT. Obviously, PC as an intermediate material in LTW PMMA/PBT can improve the weld strength of PMMA/PBT.

As is shown in Figure 10, the PC film is not completely melted. So the welding specimen of PMMA/PC/PBT can be seen as the combination of LTW PMMA/PC and PC/PBT. The weld strength of PMMA/PC/PBT stronger than the weld strength of PMMA/PBT of the weld strength is caused by the strong weld strength of PMMA/PC and PC/PBT and the detailed analysis is shown in next Sections. The weld strength of PMMA/PC/PBT is lower than the weld strength of PMMA/PC and PC/PBT. It may be caused by the laser need to through the upper two materials. In this process, the laser energy loss is more than the laser energy loss in the process of laser through the one material. Most of the PC/PBT weld strength is stronger than PMMA/PC. It may cause that the most tensile fracture of LTW PMMA/PC/PBT specimens happened in upper material.

Micro Morphology Analysis of the Weld Zone

The Figure 11 shows the micromorphology of the weld zone on the specimen of PMMA/PBT when the laser power is 17 W. The picture is magnified 400 times. Figure 11(a) shows the micromorphology of weld zone on PMMA; Figure 11(b) shows the micromorphology of weld zone on PBT. In the picture, there are many big bubbles (holes) at the interface of PMMA and PBT, and the surfaces of these bubbles are smooth.

The Figure 12 shows the micromorphology of the weld zone on the specimen of PMMA/PC/PBT when the laser power is 17 W. The picture is magnified 400 times. Figure 12(a) shows the micromorphology of weld zone on PMMA, there are some bubbles on the surface of PMMA. And there are small pieces of plastic debris on the edge of the bubbles. This can be deduced that bubbles can form the micromechanical riveting at the surface of PMMA and PC. So weld strength at the surface of PMMA and PC is higher than the weld strength at the surface of PMMA and PBT. Figure 12(b) shows the micromorphology of weld zone on PC which at the interface of PMMA and PC. Figure 12(c) shows the micromorphology of weld zone on PBT and these bubbles are smaller than others. The area of the weld seam decreases with the increasing the number of bubbles and the size of bubbles. This can reduce the weld strength. So weld strength at the surface of PC and PBT is higher than the weld strength at the surface of PMMA and PBT. The main reason for forming the bubbles is that the much thermal energy resulting the degradation of PC. These bubbles mainly consist of water vapor, carbon dioxide, carbon monoxide, and hydrocarbons.[33] Liu *et al.*[11] founded that the bubbles are good for the high weld strength in some extent. Liu *et al.*[34] studied joining of

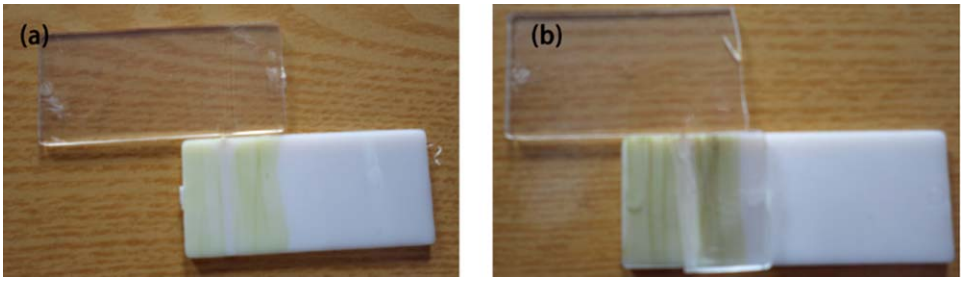

Figure 9. The broken welding specimens: (a) PMMA/PBT and (b) PMMA/PC/PBT. [Color figure can be viewed in the online issue, which is available at wileyonlinelibrary.com.]

Table III. Experimental Parameters and Results of Welding

Specimen	Laser power (W)	Weld width (mm)	Pulling force (N)	Weld strength (MPa)	Standard deviation
1	15	1.41	488.21	17.31	0.0668
2	17	1.46	532.61	18.24	0.0895
3	19	1.39	549.26	19.76	0.0738
4	21	1.41	576.73	20.45	0.0796
5	23	1.38	510.60	18.77	0.0776
6	25	1.54	475.23	15.43	0.0909
7	15	2.07	726.37	17.55	0.0852
8	17	2.12	954.50	22.51	0.0727
9	19	3.03	1215.38	20.06	0.0866
10	21	3.37	1152.09	17.09	0.0951
11	23	2.96	983.04	16.61	0.0828
12	25	2.98	967.96	16.24	0.0779
13	15	2.29	197.52	4.31	0.1128
14	17	2.65	172.78	3.26	0.0893
15	19	2.85	138.34	2.43	0.0679
16	21	3.76	186.01	2.47	0.0714
17	23	3.02	135.90	2.25	0.1141
18	25	3.56	168.66	2.37	0.0786
19	15	2.40	467.90	9.75	0.1022
20	17	2.13	421.35	9.89	0.0855
21	19	3.08	618.65	10.04	0.0939
22	21	3.02	464.37	7.69	0.0689
23	23	3.15	413.11	6.56	0.0925
24	25	3.39	328.85	4.85	0.0583

aluminum alloy to polyethylene glycol terephthalate (PET) using friction lap welding. They also discovered that these bubbles generate high pressure pushing the fused polymers to the pits and micro voids on the surface of metal, which can supply more mechanical bonding and realize tight joining between metal and polymers. So the weld strength of PMMA/PC/PBT is stronger than the weld strength of PMMA/PBT.

Rheometry

In order to facilitate the relationship between η_0 and T, the eq. (7) need to be rewritten to:

$$\ln \eta_0(T) = \ln A + \frac{B}{T} = C + \frac{B}{T} \tag{12}$$

where $C(=\ln A)$ and B are constant.

According to Figures 2–4, $\ln \eta_0$ can be determined at various temperatures by eq. (12) as plotted in Figures 13–15.

According to Figure 11, the value of B and C can be obtained. Therefore the relationship between $\ln \eta_0$ and $1/T$ can be written to:

$$\ln \eta_0(T) = -29.25 + \frac{18999.49}{T} \tag{13}$$

And the eq. (13) can be rewritten to:

$$\eta_0(T) = 0.78 \times \exp\left(\frac{18999.49}{T} - 29\right) \tag{14}$$

According to eqs. (8) and (14), reptation time for PMMA can be written to:

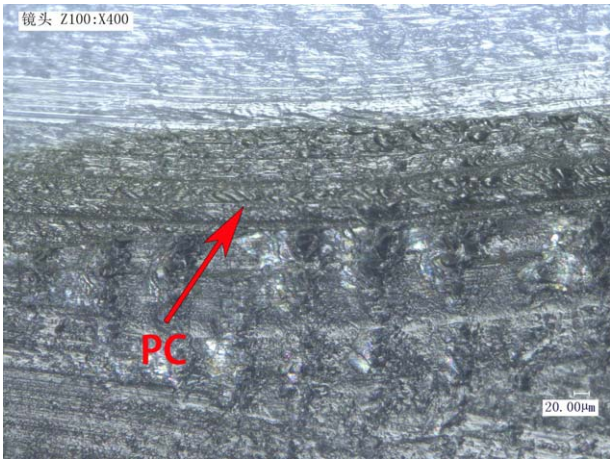

Figure 10. Cross-sectional micrograph of the welding seam. [Color figure can be viewed in the online issue, which is available at wileyonlinelibrary.com.]

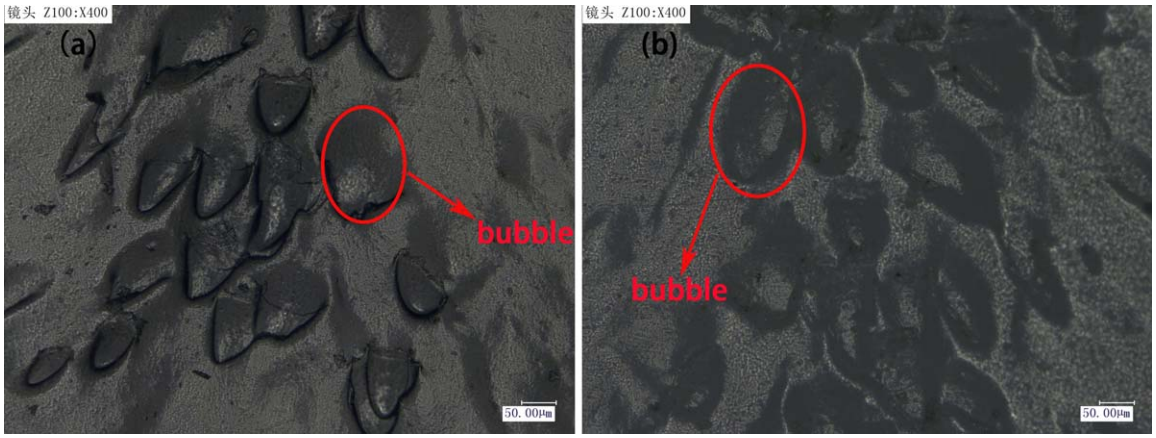

Figure 11. The micromorphology of the weld zone on the specimen of PMMA/PBT: (a) PMMA and (b) PBT. [Color figure can be viewed in the online issue, which is available at wileyonlinelibrary.com.]

$$\tau_{rep}(T) = \frac{1.68}{T} \times \exp\left(\frac{18999.49}{T} - 29\right) \quad (15)$$

Similarly, the reptation time for PC and PBT can be obtained respectively, as the eqs. 16 and 17 shows:

$$\tau_{rep}(T) = \frac{0.15}{T} \times \exp\left(\frac{14686.81}{T} - 19\right) \quad (16)$$

$$\tau_{rep}(T) = \frac{0.22}{T} \times \exp\left(\frac{14717.34}{T} - 24\right) \quad (17)$$

According to eqs. 15–17, curves of reptation time for PMMA, PC, and PBT versus temperature can be plotted in Figure 16.

Figure 16 shows curves of the reptation time for PMMA, PC, and PBT. From Figure 16, reptation times are decreased with the increase of temperature, and the decreasing speed is faster

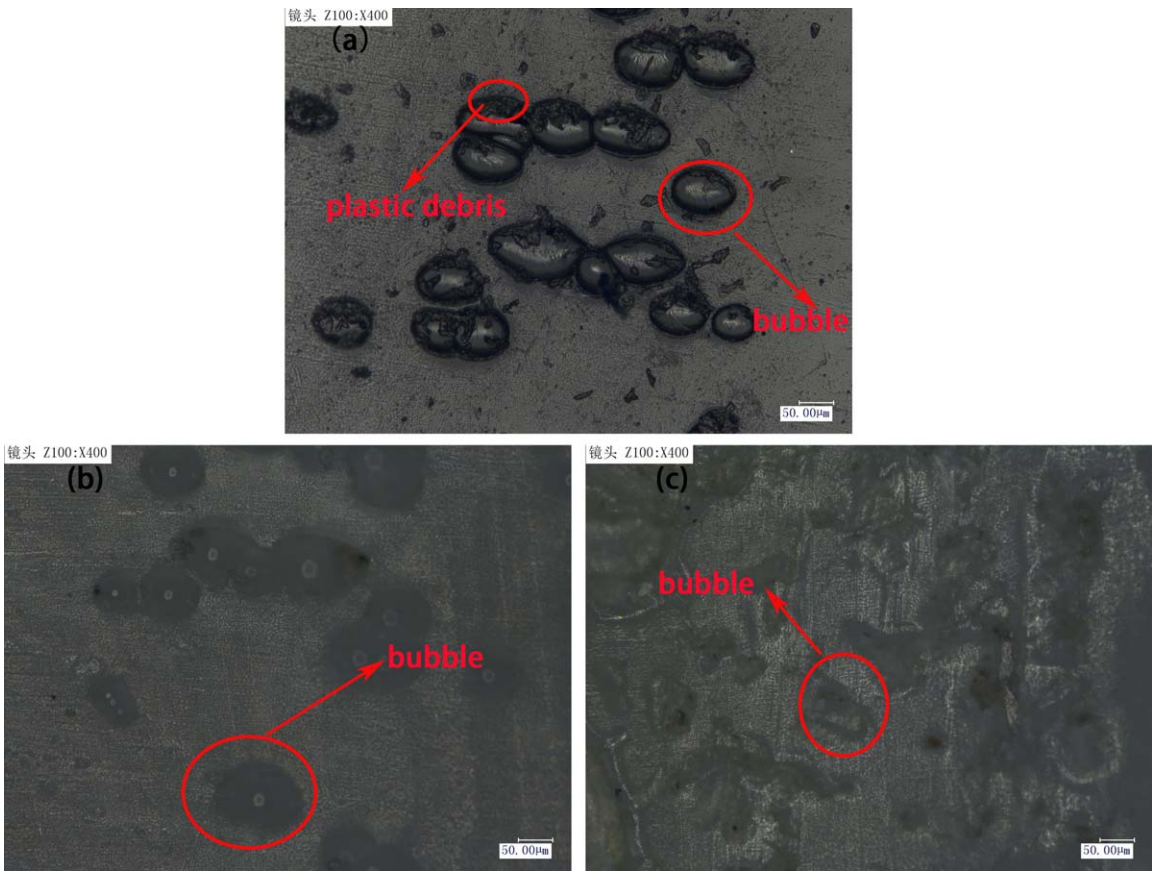

Figure 12. The micromorphology of the weld zone of the specimen of PMMA/PC/PBT: (a) PMMA; (b) PC which at the interface of PMMA and PC; and (c) PBT. [Color figure can be viewed in the online issue, which is available at wileyonlinelibrary.com.]

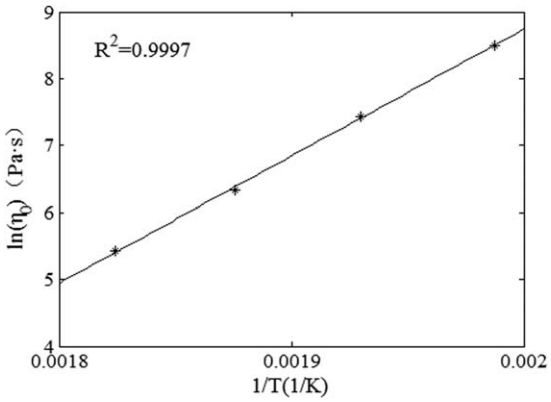

Figure 13. The linear fitting curve of ln η_0 versus $1/T$ for PMMA.

and faster, finally the reptation time tends to zero and reaches to milliseconds; the reptation time of PMMA and PC is obviously higher than the reptation time of PBT. When the temperature is at 560 K, the reptation time for PMMA, PC, and PBT are 414.2 ms, 368.4 ms, and 3.8 ms, respectively. These reptation times are under the seconds, and the reptation time for PMMA and PC are much bigger than the time for PBT. The time in molten state for LTW is reported to be in the range of seconds.[35] If the reptation time is much shorter than the process time, the higher weld strength is feasible.[29] So the weld strength of PC/PBT is stronger than the weld strength of PMMA/PC.

Equilibrium Interfacial Width

DSC was performed to evaluate the glass transition temperature (T_g) and melting temperature (T_m), and these temperatures and the data in Table II were used in eq. (2). Flory–Huggins interaction parameters can be calculated and the results of calculation are shown as follows: $\chi_{ab}=0.072$; $\chi_{bc}=0.448$; and $\chi_{ac}=0.466$, where letter a represents PMMA; letter b represents PC; letter c represents PBT. From eq. (3), the equilibrium interfacial width can be predicted to:

$$w_{\infty 12}=2\sqrt{\frac{b_1^2+b_2^2}{12\chi}}=2\times\sqrt{\frac{(6.24\,\mathrm{A})^2+(10.07\,\mathrm{A})^2}{12\times 0.072}}=25.5\,\mathrm{A}=2.55\,\mathrm{nm} \quad (18)$$

Similarly, $w_{\infty 13}=0.72$ nm; $w_{\infty 23}=2.20$ nm.

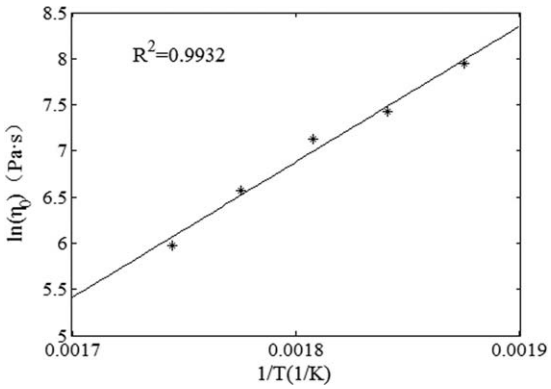

Figure 14. The linear fitting curve of ln η_0 versus $1/T$ for PC.

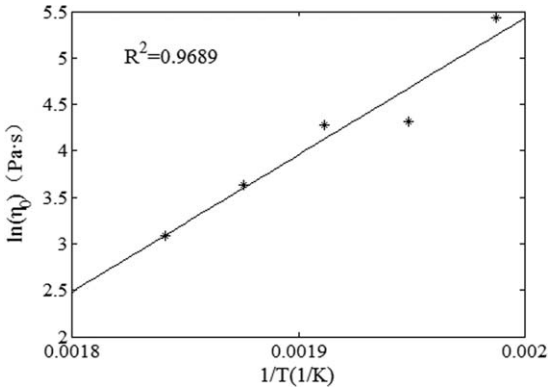

Figure 15. The linear fitting curve of ln η_0 versus $1/T$ for PBT.

Both the equilibrium interfacial width and entanglement mesh size are important for the strength development at the interface and the mesh size need to be smaller than equilibrium interfacial width to ensure entanglements. Therefore the welding ability can be reflected through w_∞/a_{max} (a_{max} is the bigger of two tube diameters).[21] Through the calculation, the w_∞/a_{max} of PMMA/PC is about 0.36; the w_∞/a_{max} of PC/PBT is about 0.10; the w_∞/a_{max} of PMMA/PBT is about 0.58. Juhl *et al.*[21] calculated results of w_∞/a_{max} with Hansen equation: the w_∞/a_{max} of PMMA/PC is about 0.29; the w_∞/a_{max} of PBT/PC is about 0.26; the w_∞/a_{max} of PMMA/PBT is about 0.10. The reason for the difference of two results is the difference of absolute temperature in calculating χ, (the related temperature of materials which measured by Juhl are that the T_g of PMMA is 383.24 K, the T_g of PC is 422.86 K and T_m of PBT is 495.09 K). From above, the molecule chain entanglements can be completed at the welding interfaces of PMMA/PC, PC/PBT, and two groups of materials have good compatibility; Molecular chain entanglement can rarely be completed at the welding interface of PMMA/PBT, so this group materials has poor compatibility. Therefore the welding performance of PMMA/PBT is relatively poor, and adding PC film as intermediate can improve the weld strength of PMMA/PBT.

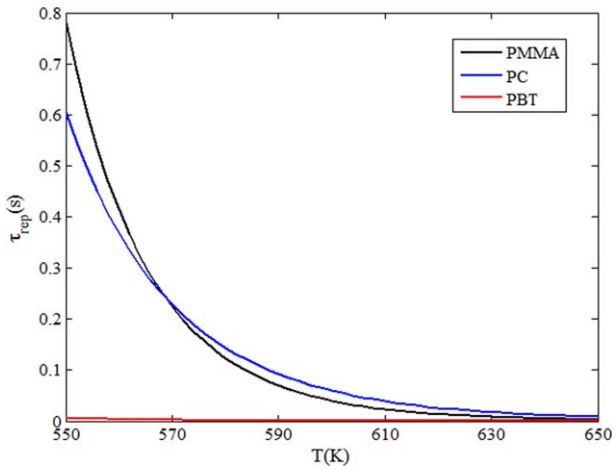

Figure 16. The reptation time of PMMA, PC, and PBT versus temperature. [Color figure can be viewed in the online issue, which is available at wileyonlinelibrary.com.]

Table IV. Process Control Parameters and Their Limits

		Limits				
Parameter	Notation	−2	−1	0	1	2
Laser power (W)	*P*	15	17	19	21	23
Welding speed (mm/s)	*S*	2	3	4	5	6
Clamping pressure (MPa)	*C*	0.4	0.45	0.5	0.55	0.6

MATHEMATICAL MODELING WITH RSM

Experimental Design

In this study, three key process parameters that determined the quality of the LTW process were laser power (*P*), welding speed (*S*), and clamping pressure (*C*). The experiment was designed on the basis of a three-factor five-level central composite design (CCD), with full replication. One response is weld strength as output variable. The statistical software Design-Expert version 8 was used to conduct statistical analysis, develop mathematical models, and optimize the process parameters. The selected process parameters and their limits, units and notations are listed in Table IV. The CCD matrix of the variables and their corresponding results are listed in Table V. In Table V, the weld strength was calculated from the tensile tests and weld seams, and the weld strength is the middle value of the five experiments. As shown in Table V, the maximum weld strength is 11.37 MPa.

RESULTS AND DISCUSSION

Development of the Mathematical Model

For weld strength, the fit summary suggests the quadratic relationship where the additional terms are significant and the model is not aliased. The analysis of variance (ANOVA) table of quadratic model is given in Table VI. As is shown in Table VI, the *P*-value less than 0.05 for the model indicates that the model terms are significant.[19] The lack-of-fit value of model indicates non-significance, as this is desirable. The laser power (*P*), welding speed (*S*), clamping pressure (*C*), the quadratic effect of the laser power (P^2), welding speed (S^2), and clamping pressure (C^2) along with the interaction effect of laser power and welding speed (*PS*), laser power and clamping pressure (*PC*), welding speed and clamping pressure (*SC*) are the significance model terms associated with weld strength. In addition, the other adequacy measures, R^2, adjusted R^2, and predicted R^2, of the responses are all in reasonable agreement and were close to 1; this indicated the adequacy of the models.[36]

The final mathematical model for weld strength, which can be used for prediction within the limited factors considered in this study, is given as follows:

a. Final equation in terms of coded factors:

$$\text{Weld strength} = 10.14 - 1.10P - 0.40S + 0.15C - 0.087PS + 0.18PC + 0.24SC - 0.33P^2 + 6.705\times10^{-3}S^2 - 0.25C^2 \quad (19)$$

b. Final equation in terms of actual factors:

$$\text{Weld strength} = -11.3097 + 1.91631P - 2.01864S + 50.31818C - 0.04375PS + 1.77500PC + 4.80000SC - 0.083636P^2 + 6.70455\times10^{-3}S^2 - 100.31818C^2 \quad (20)$$

Validation of the Developed Model

To validate the developed RSM models, three confirmation tests chosen randomly from the experimental results were conducted. The process parameters used for experiments are all with in the Table IV. Table VII shows the predicated values, actual results and calculated percentage errors of the confirmation tests. The weld strength of actual value is the middle value of the five experiments. It is observed that the predicated values of responses were in good agreement with actual results, which illustrated that the results of the developed RSM model were nearly accurate.

Figure 17 shows the relationship between the predicted and actual values of weld strength. The results illustrate that the developed RSM model of weld strength is adequate as

Table V. Design Matrix and Measured Responses

Number	*P* (W)	*S* (mm/s)	*C* (MPa)	Weld strength (MPa)
1	19	4	0.50	10.16
2	21	3	0.45	8.76
3	15	4	0.50	10.86
4	17	5	0.45	10.27
5	17	5	0.55	10.69
6	23	4	0.50	6.7
7	19	4	0.40	8.71
8	19	2	0.50	11.05
9	21	5	0.45	7.54
10	17	3	0.55	10.6
11	19	4	0.50	10.13
12	21	3	0.55	8.93
13	19	4	0.50	10.28
14	17	3	0.45	11.37
15	19	4	0.50	10.14
16	19	4	0.50	10.02
17	19	4	0.50	10.05
18	19	6	0.50	9.24
19	21	5	0.55	8.44
20	19	4	0.60	9.52

Table VII. Validation Test Results

Number	*P* (W)	*S* (mm/s)	*C* (MPa)		Weld strength (MPa)
1	16	3	0.55	Actual	11.17
				Predicted	11.44
				(Error) %	2.42
2	18	4	0.50	Actual	9.86
				Predicted	10.60
				(Error) %	7.51
3	20	5	0.45	Actual	8.09
				Predicted	8.34
				(Error) %	3.09

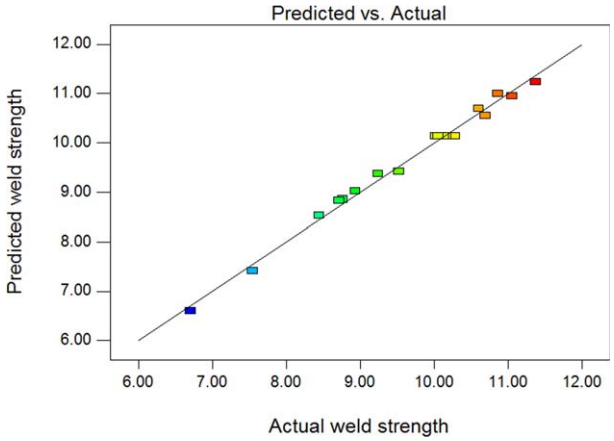

Figure 17. The relationship between the predicted and actual values of weld strength. [Color figure can be viewed in the online issue, which is available at wileyonlinelibrary.com.]

percentage error between predicted and actual value, which the developed model of weld strength is accurate.

Effects of Process Parameters on the Weld Strength

Figure 18(a,b) shows the interaction effect of laser power and welding speed on weld strength when clamping pressure is 0.5 MPa. The weld strength tends to increase with slow welding speed and low laser power when the process parameters are within a certain range (*P*: 15–23 W; *S*: 2–7 mm/s). When the power is large, the weld strength is low. It may be caused by the excessive laser energy input, which leads to a large amount of degradation or ablation of the material. Usually, the greater the laser energy and the smaller the welding speed can cause the greater the energy input. In this study, when the laser power and welding speed are smaller, the weld strength is higher. It indicated that the laser power is more important than welding speed in interaction effect of laser power and welding speed on weld strength.

Figure 19(a,b) shows the interaction effect of laser power and clamping pressure on weld strength when welding speed is 4 mm/s. The weld strength tends to increase with low laser power and the clamping pressure up to the center, when the process parameters are within a certain range (*P*: 15–23 W; *C*: 0.4–0.6 MPa). When the clamping pressure is too big, the molecular mobility of materials becomes poor; when clamping is too small, the materials at interface of welding seam cannot be fully contacted, and the heat conduction efficiency is declined. These may be caused the high weld strength occurs when the clamping pressure up to the center.

Table VI. ANOVA

Source	Sum of squares	df	Mean squares	*F* value	*P* value	
Model	26.93	9	2.99	130.38	<0.0001	Significant
P	19.32	1	19.32	841.53	<0.0001	
S	2.51	1	2.51	109.45	<0.0001	
C	0.34	1	0.34	14.91	0.0032	
PS	0.061	1	0.061	2.67	0.1334	
PC	0.25	1	0.25	10.98	0.0078	
SC	0.46	1	0.46	20.08	0.0012	
P^2	2.81	1	2.81	122.60	<0.0001	
S^2	1.130×10^{-3}	1	1.130×10^{-3}	0.049	0.8289	
C^2	1.58	1	1.58	68.90	>0.0001	
Residual	0.23	10	0.023			
Lack of fit	0.19	5	0.038	4.47		Not significant
Pure error	0.042	5	8.400×10^{-3}			
Cor total	27.16	19				
	Standard deviation = 0.15				R^2 = 0.9915	
	Mean = 9.67				Adjusted R^2 = 0.9839	
	Coefficient of variation = 1.57				Predicted R^2 = 0.9414	
	Predicted residual error of sum of squares = 1.59				Adequate precision = 43.273	

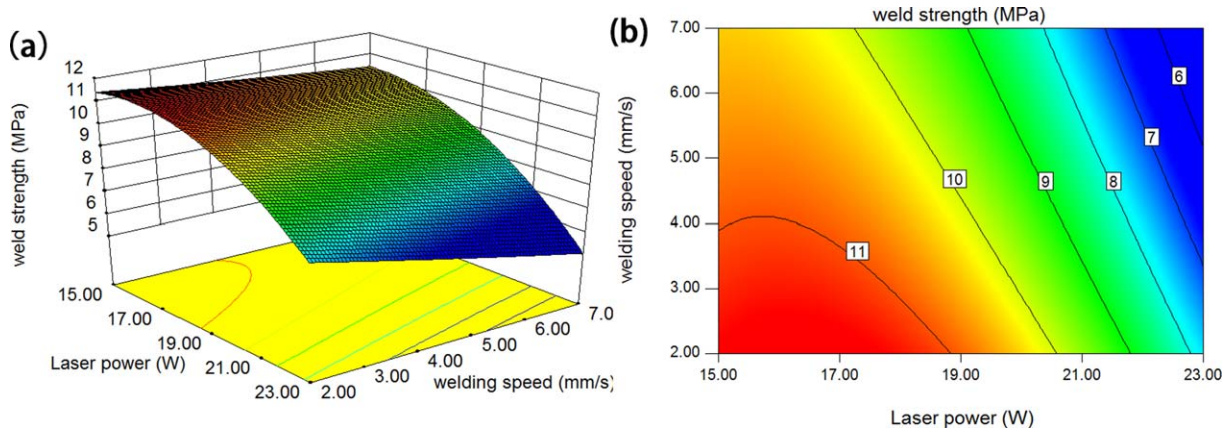

Figure 18. Interaction effect of laser power and welding speed on weld strength: (a) the response surface plot and (b) the contour plot. [Color figure can be viewed in the online issue, which is available at wileyonlinelibrary.com.]

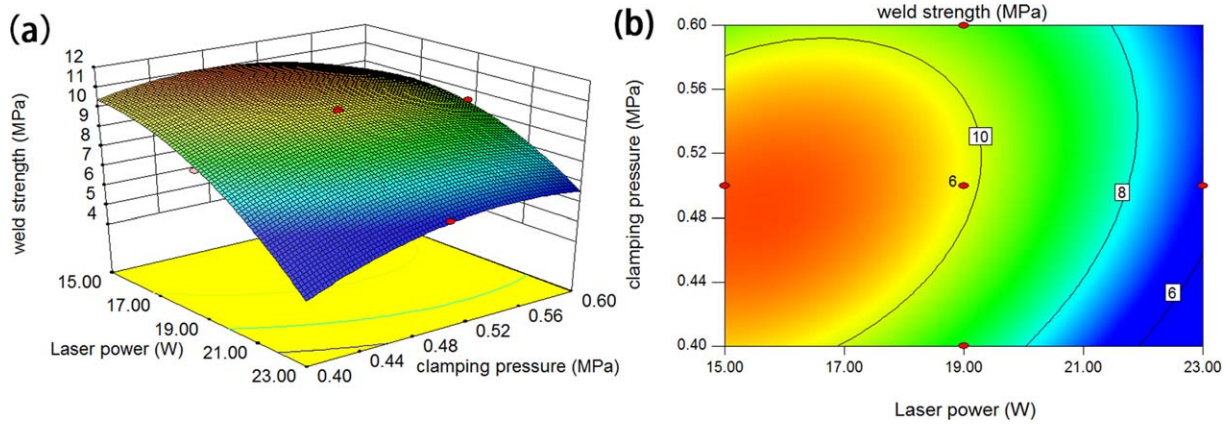

Figure 19. Interaction effect of laser power and clamping pressure on weld strength: (a) the response surface plot and (b) the contour plot. [Color figure can be viewed in the online issue, which is available at wileyonlinelibrary.com.]

Figure 20(a,b) shows the interaction effect of welding speed and clamping pressure on weld strength when laser power is 18 W. The weld strength tends to increase with slow welding speed and clamping pressure up to center when the process parameters are within a certain range (*S*: 2–7 mm/s; *C*: 0.4–0.6 MPa).

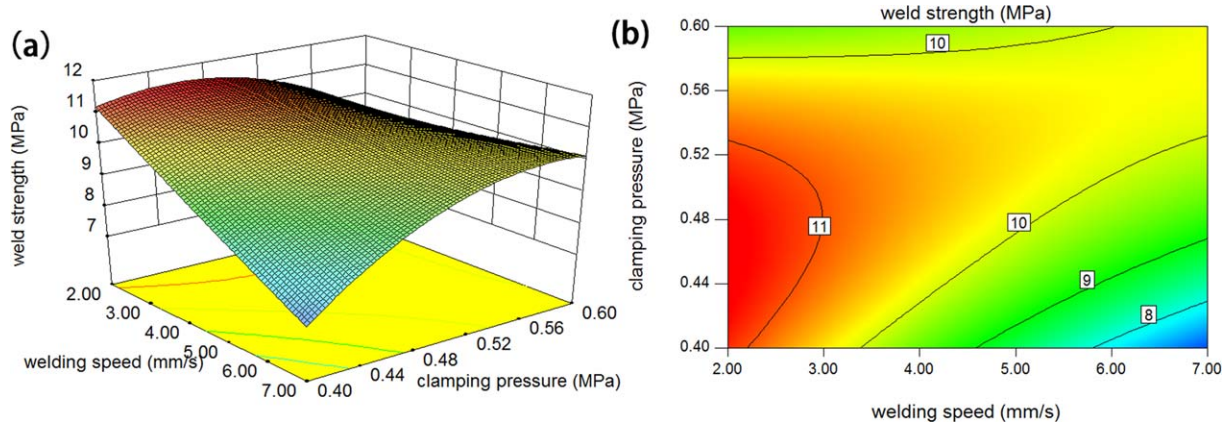

Figure 20. Interaction effect of welding speed and clamping pressure on weld strength: (a) the response surface plot and (b) the contour plot. [Color figure can be viewed in the online issue, which is available at wileyonlinelibrary.com.]

CONCLUSIONS

In this article, the PC film as intermediate material was used to enhance weld strength in LTW of PMMA and PBT and the welding mechanism was studied. The conclusions show that:

1. In the LTW of PMMA and PBT, when the laser power is 19 W, the weld strength of specimens with PC film is more than four times stronger than the weld strength of specimens without PC film; under other conditions, the weld strength of specimens with PC film is about two to four times stronger than the weld strength of specimens without PC film.
2. Comparing the weld strength of PMMA/PC, PC/PBT, PMMA/PBT, and PMMA/PC/PBT, it concluded that the stronger weld strength of LTW, PMMA, and PBT with PC film may be caused by the stronger weld strength of LTW, PMMA/PC, and PC/PBT.
3. From the microperspective, the bubbles at weld zone of LTW, PMMA, and PBT with PC film are much more than LTW, PMMA, and PBT without PC film. These bubbles are used to form the micromechanical riveting to enhance the weld strength.
4. When the temperature is at 560 K, the reptation time was determined as 414.2 ms, 368.4 ms, and 3.8 ms for PMMA, PC, and PBT, respectively. When the reptation time is much shorter than time in molten state, the higher weld strength is feasible. It can be concluded that the weld strength of PC/PBT is higher than the weld strength of PMMA/PC.
5. The relationship between equilibrium interfacial width and tube diameter play an important role in the development of weld strength. The equilibrium interfacial width need to close to the tube diameter to ensure the entanglements. From this it is to conclude that equilibrium interfacial width was concluded to 2.55 nm, 2.20 nm, and 0.72 nm for PMMA/PC, PC/PBT, and PMMA/PBT, respectively. The equilibrium interfacial width for PMMA/PBT is much shorter than tube diameters for PMMA and PBT; so the compatibility of PMMA and PBT is poor. While the former two equilibrium interfacial widths are close to the tube diameters for PMMA, PC and PBT; thus, the entanglements can form and PC has good compatibility with PMMA and PBT. That is the reason for the weld strength enhancement.
6. Decreasing the laser power and welding speed increases the weld strength, and the laser power is more important than welding speed in interaction effect of laser power and welding speed on weld strength; the clamping pressure up to the center increases the weld strength.
7. The developed mathematical model in this study can predict the responses adequately within the limits of welding parameters being used, which concluded from validation experiments that the estimated results are in good agreement with the measured data.

ACKNOWLEDGMENTS

The authors acknowledge the National Natural Science Foundation of China (grant number 51275219), College Students' Innovation Practice Fund of Industry center in Jiangsu University (ZXJG201593).

REFERENCES

1. Ingo, B.; Ulrich, A. R.; Hans, J. H. *SPIE* **2004**, *5339*, 454.
2. Amanat, N.; Chaminade, C.; Grace, J. *Mater. Des.* **2010**, *31*, 4823.
3. Haberstroh, E.; Luzeler, R. *ANTEC* **2003**, *1099*.
4. Kolesnikov, B.; Herbeck, L.; Fink, A. *Compos. Struct.* **2008**, *84*, 368.
5. Wang, X.; Chen, H.; Liu, H. X. *Mater. Des.* **2014**, *55*, 343.
6. Sokolowski, W.; Bruns, P. *ICALEO* **2004**, 205.
7. Seiji, K.; Yousuke, K. *Script. Mater.* **2008**, *59*, 1247.
8. Anssi, J.; Saara, K.; Antti, S. *ICALEO* **2003**, *95*, 124.
9. Aden, M.; Otto, G.; Duwe, C. *Int. Polym. Proc.* **2013**, *28*, 300.
10. Acherjee, B.; Kuar, A. S. *Lasers Manuf. Mater. Process.* **2015**, *2*, 103.
11. Liu, H. X.; Jiang, H. R.; Guo, D. H. *Materials* **2015**, *8*, 4961.
12. Liu, H. X.; Chen, G. C.; Jiang, H. R. *J. Appl. Polym. Sci.* **2016**, *133*, DOI: 10.1002/app.43068.
13. Farzad, A.; Mohamadreza, A.; Jamshid, A. *Mater. Des.* **2015**, *65*, 473.
14. Fu, N.; Li, G. H.; Wang, N. Y. *Mater. Des.* **2015**, *87*, 495.
15. Won, H. J.; Joo, Y. K.; Moo, S. L. *Polym. J.* **1994**, *26*, 465.
16. Vijay, K. S. *J. Adhes. Sci. Technol.* **2001**, *15*, 57.
17. Qiu, J. H.; Zhong, G. H.; Asao, M. *Int. J. Adhes. Adhes* **2010**, *30*, 729.
18. Vijay, K. S. *Polymer* **1998**, *39*, 2469.
19. Montgomery, D. C. Design and Analysis of Experiments, 6th ed.; Wiley: New York, **2001**.
20. Bower, D. I. An Introduction to Polymer Physics; Cambridge University Press: Cambridge, **2002**.
21. Juhl, T. B.; Bach, D.; Larson, R. G. *Polymer* **2013**, *54*, 3891.
22. Hansen, C. M. Hansen Solubility Parameters—a User's Handbook, 2nd ed.; Florida, USA: CRC Press, **2000**.
23. Cowie, J. M. G.; Arrighi, V. Polymers—Chemistry and Physics of Modern Materials.; Florida, USA: CRC Press, **2007**.
24. Lo, C. T.; Narasimhan, B. *Polymer* **2005**, *46*, 2266.
25. Helfand, E.; Sapse, A. M. *J. Chem. Phys.* **1975**, *62*, 1327.
26. Dealy, J. M.; Larson, R. G. Structure and Rheology of Molten Polymers—From Structure to Flow Behavior and Back Again; Hanser Publishers: Munich, Germany, **2006**.
27. Gennes, P. G. D. *J. Chem. Phys.* **1971**, *55*, 572.
28. Wool, R. P. Polymer Interfaces—Structure and Strength; Hanser Publishers: Munich, **1995**.
29. Juhl, T. B.; Christiansen, J. D.; Jensen, E. A. *J. Appl. Polym. Sci.* **2013**, *129*, 2679.
30. Doi, M. Introduction to Polymer Physics; Clarendon Press: Oxford, **1996**.

31. Fetters, L. J.; Lohse, D. J.; Colby, R. H. Chain Dimensions and Entanglement Spacings; Springer: New York, **2007**.
32. Toyonaka. *Macromolecules* **1976**, *9*, 266.
33. Braun, E.; Levin, B. C. *Fire Mater.* **1987**, *11*, 71.
34. Liu, F. C.; Liao, J.; Nakata, K. *Mater. Des.* **2014**, *54*, 236.
35. Mayboudi, L. S.; Birk, A. M.; Zak, G. *J. Laser Appl.* **2010**, *22*, 22.
36. Acherjee, B.; Misra, D.; Bose, D.; Venkadeshwaran, K. *J. Opt. Laser Technol.* **2009**, *41*, 956.